Electronic Supplementary Material (ESI) for Nanoscale.

Reprogrammable Multifunctional Chalcogenide Guided-wave Lens

Tun Cao*[,a], Chen-Wei Wei[a], Meng-Jia Cen[a], Bao Guo[a], Yong-June Kim[b], Shuang Zhang[c] and Cheng-Wei Qiu*[,b]

[a]School of Optoelectronic Engineering and Instrumentation Science, Dalian University of Technology, 116024, China

[b]Department of Electrical and Computer Engineering, National University of Singapore, 4 Engineering Drive 3, Singapore 117583, Republic of Singapore

[c]School of Physics and Astronomy, University of Birmingham, Birmingham B15 2TT, UK

*Corresponding Author: E-mail: chengwei.qiu@nus.edu.sg; caotun1806@dlut.edu.cn

Section 1. Derivation of the refractive index profile of the curvature

As can be observed in the right column of Fig.1b, the curved surface *S* is produced by rotating a curve *C* symmetrically about the *z*-axis. The other two cylindrical coordinates are *ρ* and *ϑ*. Herein, we specify the curve *C* and thus the surface *S* by providing *ρ*(*s*) or *s*(*ρ*) where *s* is the arc distance measured along the *C*. One could use as the surface coordinates either *s* and *ϑ* or, on occasions, *ρ* and *ϑ*. The surface metric that gives the distance *dL* between the neighboring points is shown by

$$dL^2 = ds^2 + \rho^2 d\theta^2 \qquad \text{* MERGEFORMAT (S1)}$$

If we multiply the *dL* by *n*, the refractive index and optical distance $\mathrm{d}\zeta$ between the neighboring points can be expressed by

$$\mathrm{d}\zeta^2 = n^2\left(ds^2 + \rho^2 d\theta^2\right) \qquad \text{* MERGEFORMAT (S2)}$$

If *s* and *ϑ* are treated as the independent variables, Eq. (S2) may be rewritten as

$$\mathrm{d}\zeta^2 = n(s)^2\left(ds^2 + \rho(s)^2 d\theta^2\right) \qquad \text{* MERGEFORMAT (S3)}$$

However, if *ρ* and *ϑ* are chosen, it can be alternatively written as

$$\mathrm{d}\zeta^2 = N(\rho)^2\left(s'(\rho)^2 d\rho^2 + \rho^2 d\theta^2\right) \qquad \text{* MERGEFORMAT (S4)}$$

where *N(ρ)=n(s)*. If we employ the bars over the quantities to present those relating to a particular structure and unbarred quantities for those associated with other equivalent structure[34] , the equivalence of the optical metrics, by Eq.(s2), requires

$$n^2\left(ds^2 + \rho^2 d\theta^2\right) = \bar{n}^2\left(d\bar{s}^2 + \bar{\rho}^2 d\bar{\theta}^2\right) \qquad \text{* MERGEFORMAT (S5)}$$

where $n ds = \bar{n} d\bar{s}$, $n\rho = \bar{n}\bar{\rho}$, and $\theta = \bar{\theta}$. It thus results in the behind set of integral relationships,

$$\int_a^s n ds = \int_{\bar{a}}^{\bar{s}} \bar{n} d\bar{s} \qquad \text{* MERGEFORMAT (S6)}$$

$$n\rho = \bar{n}\bar{\rho} \qquad \text{* MERGEFORMAT (S7)}$$

$$\int_b^s ds/\rho = \int_{\bar{b}}^{\bar{s}} d\bar{s}/\bar{\rho} \qquad \text{* MERGEFORMAT (S8)}$$

where *a* and $\bar{a}$, *b* and $\bar{b}$ show the values of *s* and $\bar{s}$ corresponding to the equal points in the two guides[34]. We can then determine $\bar{n}(\bar{s})$ and $\bar{\rho}(\bar{s})$ when they correspond to the given guide. The mapping function $\bar{s} = f(s)$ can be achieved by solving Eq. (S8) for $\bar{s}$. By setting $\bar{s} = \bar{\rho} = r$ for a flat guide, Eqs. (S7) and (S8) are derived as following Eqs. (S9) and (S10), respectively.

$$N\rho = n(r)r$$ * MERGEFORMAT (S9)

$$\int_b^s ds/\rho = \int_1^r dr/r = \ln r$$ * MERGEFORMAT (S10)

Thus the mapping function is

$$r = f(s) = \exp\int_b^s ds/\rho$$ * MERGEFORMAT (S11)

where *s*=*b* corresponds to *r*=1. One can derive below Eq. (S12) using Eqs. (S9) and (S11).

$$N(s) = n\left[f(s)\right]f(s)/\rho(s)$$ * MERGEFORMAT (S12)

If one employs *ρ* as the independent variable in place of *s* in Eq. (s11), we can then have

$$F(\rho) = \exp\int_1^{\rho}\left[s^{'}(\rho)/\rho\right]d\rho$$ * MERGEFORMAT (S13)

By replacing *f(s)* in Eq. (S12) with Eq.(S13), the refractive index of the curved surface can be derived as

$$N(\rho) = n\left[F(\rho)\right]F(\rho)/\rho$$ * MERGEFORMAT (S14)

The left-hand side of Eq. (S14) can be applied to the arbitrary rotationally symmetric curved surface on which light can propagate. We take an example of a Rinehart-shaped surface of which the arc distance *s* can be expressed as $s = \frac{1}{2}\rho + \frac{1}{2}\sin^{-1}\rho$. An analytical solution of Eq. (S14) regarding the Rinehart-shaped surface can be expressed as

$$N(\rho) = \frac{2}{\left(1+\sqrt{1-\rho^2}\right)^{\frac{1}{2}}\left(e^{\frac{\rho}{\left(1+\sqrt{1-\rho^2}\right)^{\frac{1}{2}}}} + e^{\frac{-\rho}{\left(1+\sqrt{1-\rho^2}\right)^{\frac{1}{2}}}}\right)}$$ * MERGEFORMAT (S15)

The proposed approach allows gradient index lenses to be mapped onto arbitrary rotationally symmetric curved surfaces to manipulate the wavefront of the guided-wave and thus enabling various singular phenomenon. Examples of Einstein's ring, invisible cloak, Maxwell fish-eye, and Luneburg lenses are demonstrated, for Rinehart-shaped surfaces, always leading to the requirements of isotropic permittivity. The structure is simulated by a commercial software COMSOL based on the finite element method. The computational domain has a perfect electric conductor (PEC) boundary for the top and bottom surfaces of the curvature and scattering boundary conditions around the edge. The cylindrical wave is excited by a point source, propagating from left to right with the *E*-field polarized along the z-axis.

Section 2. Refractive index of the $Ge_2Sb_2Te_5$ at the different structural phase

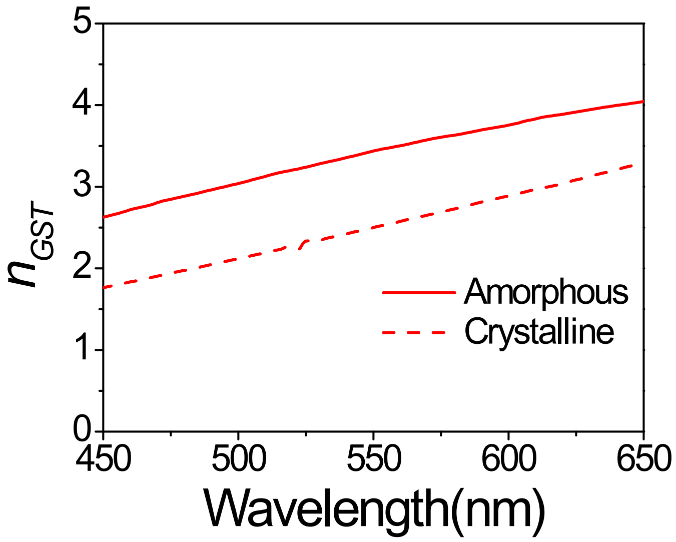

Figure S1. Refractive index nGST vs wavelength for both amorphous and crystalline phases of $Ge_2Sb_2Te_5$[27].

Section 3. "On/Off" state of the multi-functions in the Rinehart-shaped surface

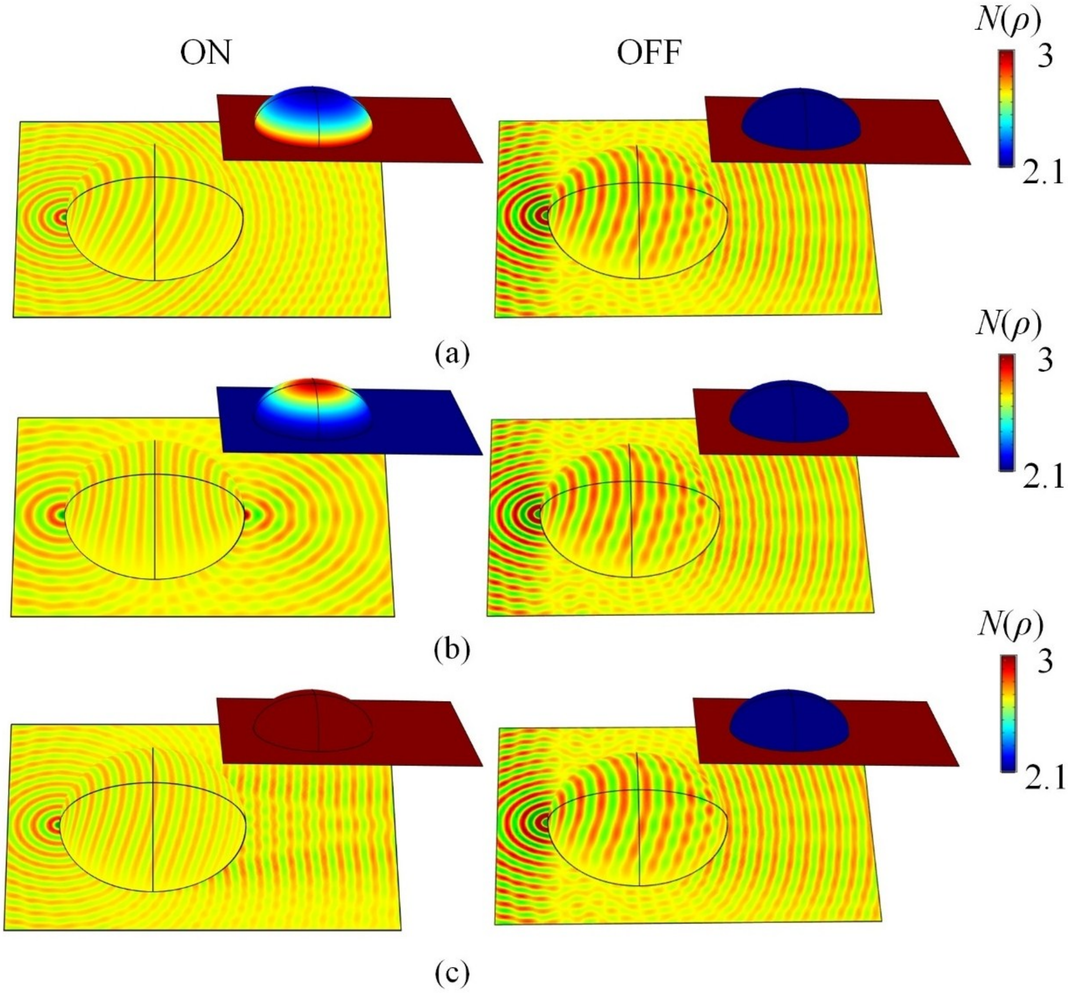

Figure S2. The left (right) columns show "on (off)" state of the functions of (a) invisible cloaking, (b) Maxwell fish-eye lens, and (c) Luneburg lens achieved by the Rinehart-shaped surface consisting of the $Ge_2Sb_2Te_5$ dielectric with the refractive index distributions presented in the insets accordingly. The right columns show that the guided-wave fronts are severely distorted once the $Ge_2Sb_2Te_5$ curvature is homogenously crystallized thus switches off the functionalities accordingly.

Section 4. The multi-functions in the Rinehart-shaped surface with the different discretization process

To explore the effect of the number of $Ge_2Sb_2Te_5$ segments on the phenomenon of Einstein ring, Figure S3 illustrates the propagation of the incident wave (λ=500 nm) across the curvatures that are divided into 6, 9, 12 and 15 slabs respectively. As can be observed, even the basic discretization of the required index profile (6-layered structure) can collimate the guided-wave. Thus, our design demonstrates an excellent tolerance of fabrication. The effect of the number of the $Ge_2Sb_2Te_5$ segments on the other functions can be found in Figs.S4-S6.

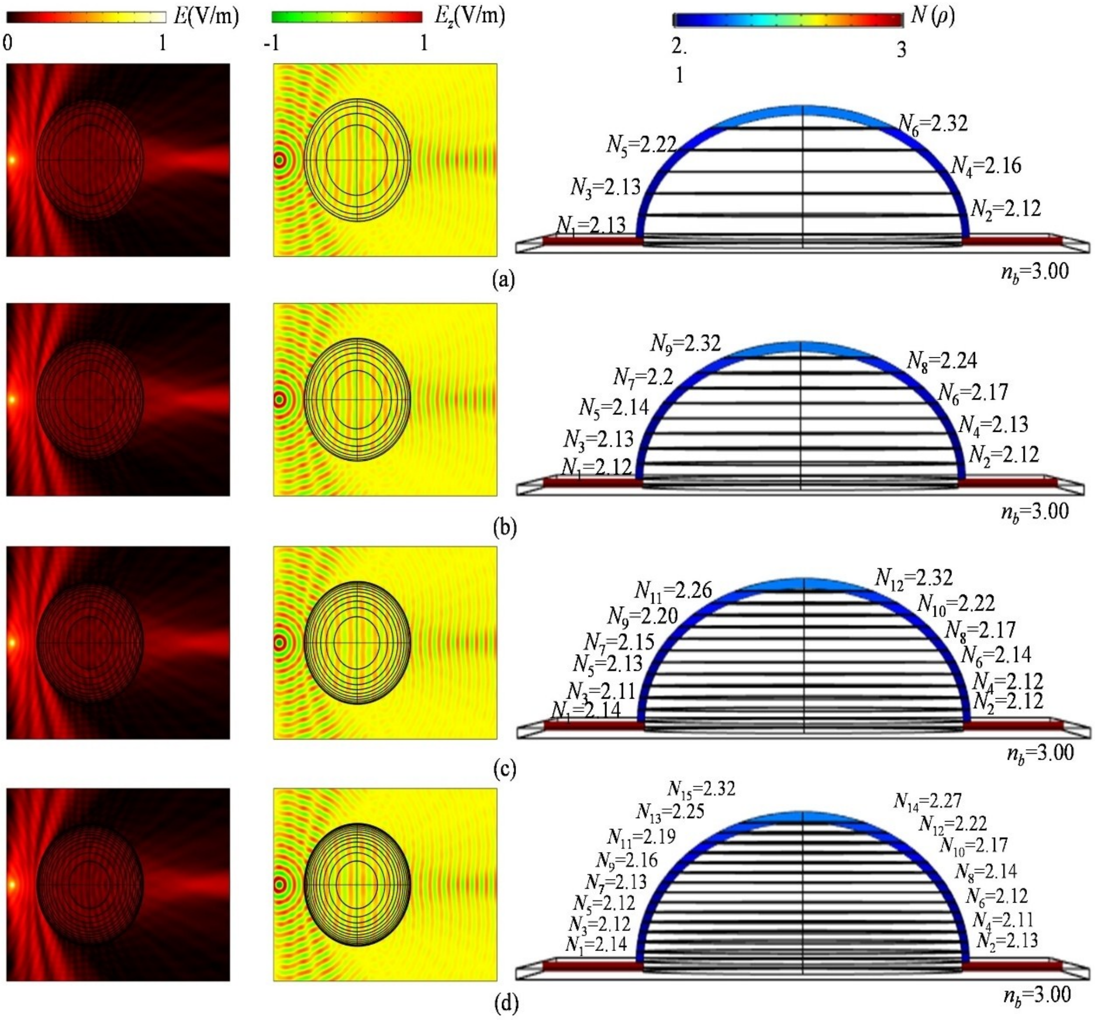

Figure S3. The propagation of E (left column) and E_z (central column) through the surface of (a) 6-layered, (b) 9-layered, (c) 12-layered, and (d) 15-layered Rinehart-shaped curvature at λ= 500 nm, where the Einstein's ring phenomenon is imitated. The radial cross sections of the different discretization process are illustrated in the right columns.

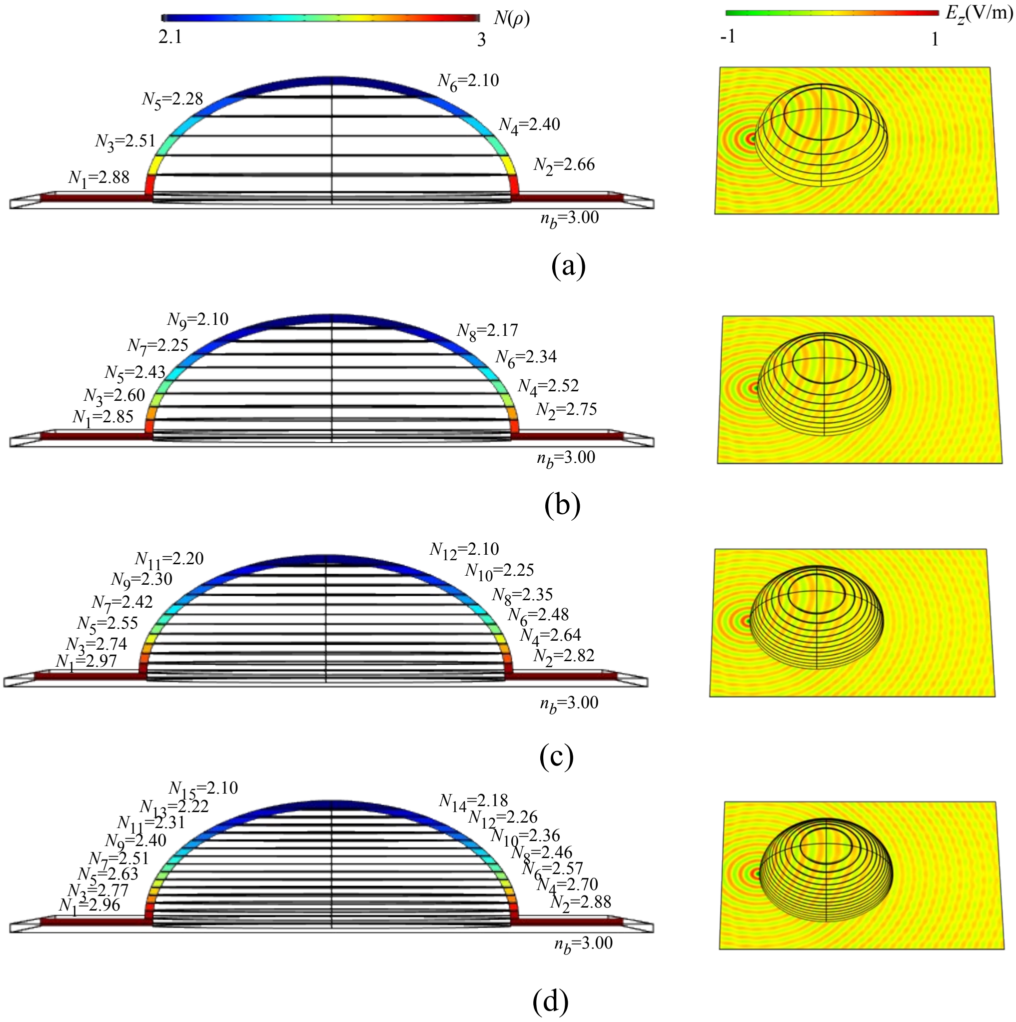

Figure S4. The propagation of E_z (right column) through the surfaces of (a) 6-layered, (b) 9-layered, (c) 12-layered, and (d) 15-layered Rinehart-shaped curvature at λ= 500 nm, where the optical invisibility phenomenon is imitated. The radial cross sections of the different discretization process are shown in the left columns.

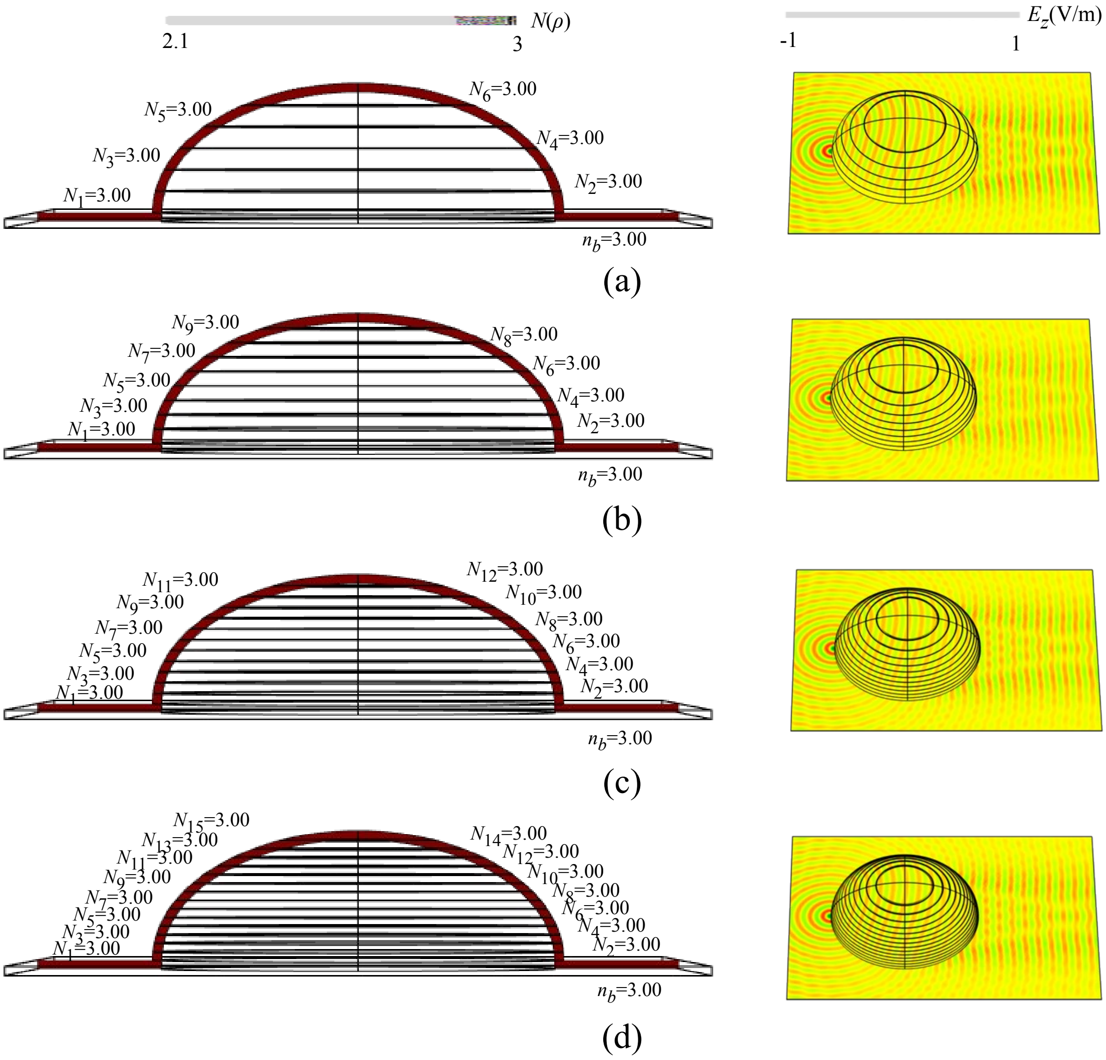

Figure S5. The propagation of E_z (right column) through the surfaces of (a) 6-layered, (b) 9-layered, (c) 12-layered, and (d) 15-layered Rinehart-shaped curvature at λ= 500 nm, where the Luneburg lens is imitated. The radial cross sections of the different discretization process are illustrated in the left columns.

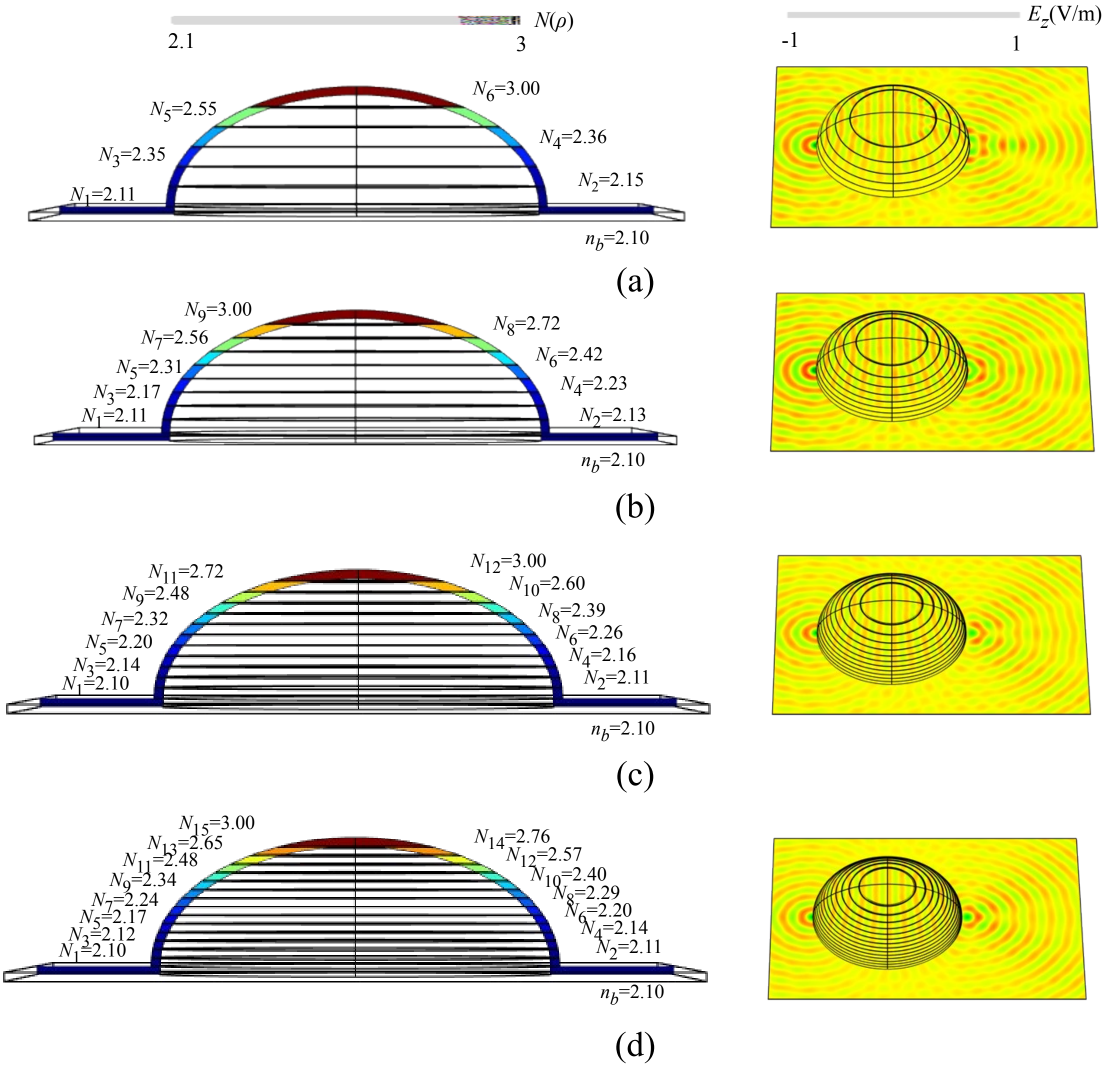

Figure S6. The propagation of E_z (right column) through the surfaces of (a) 6-layered, (b) 9-layered, (c) 12-layered, and (d) 15-layered Rinehart-shaped curvature at λ= 500 nm, where the Maxwell fish eyes lens is imitated. The radial cross sections of the different discretization process are illustrated in the left columns.

Section 5. The multi-functions in the Rinehart-shaped surface at the different wavelengths

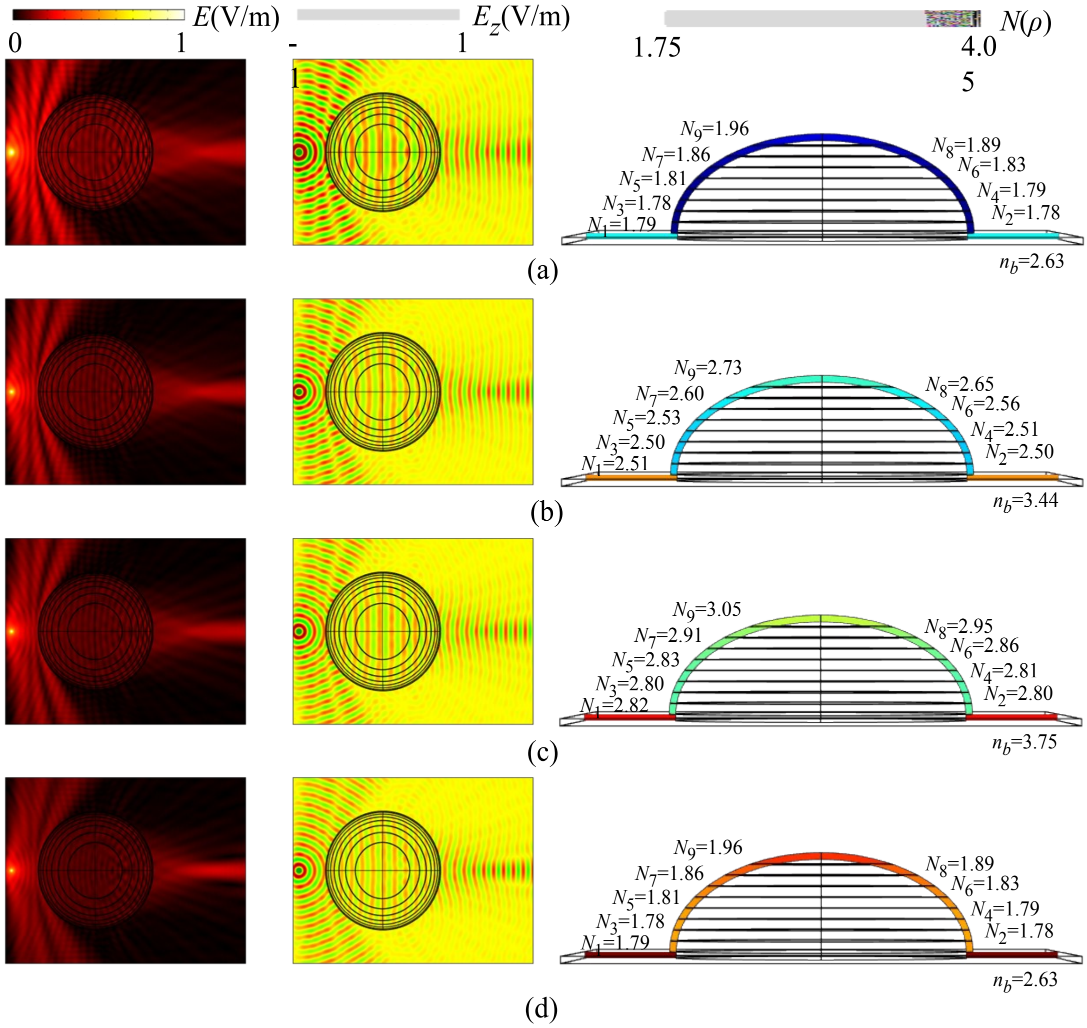

Figure S7. The propagation of *E* (left column) and E_z (central column) through the surface of 9-layered Rinehart-shaped curvature at (a) λ= 450 nm, (b) λ= 550 nm, (c) λ= 600 nm, and (d) λ= 650 nm, where the Einstein ring phenomenon is imitated. The radial cross sections of the structure at the different wavelengths are shown in the right column.

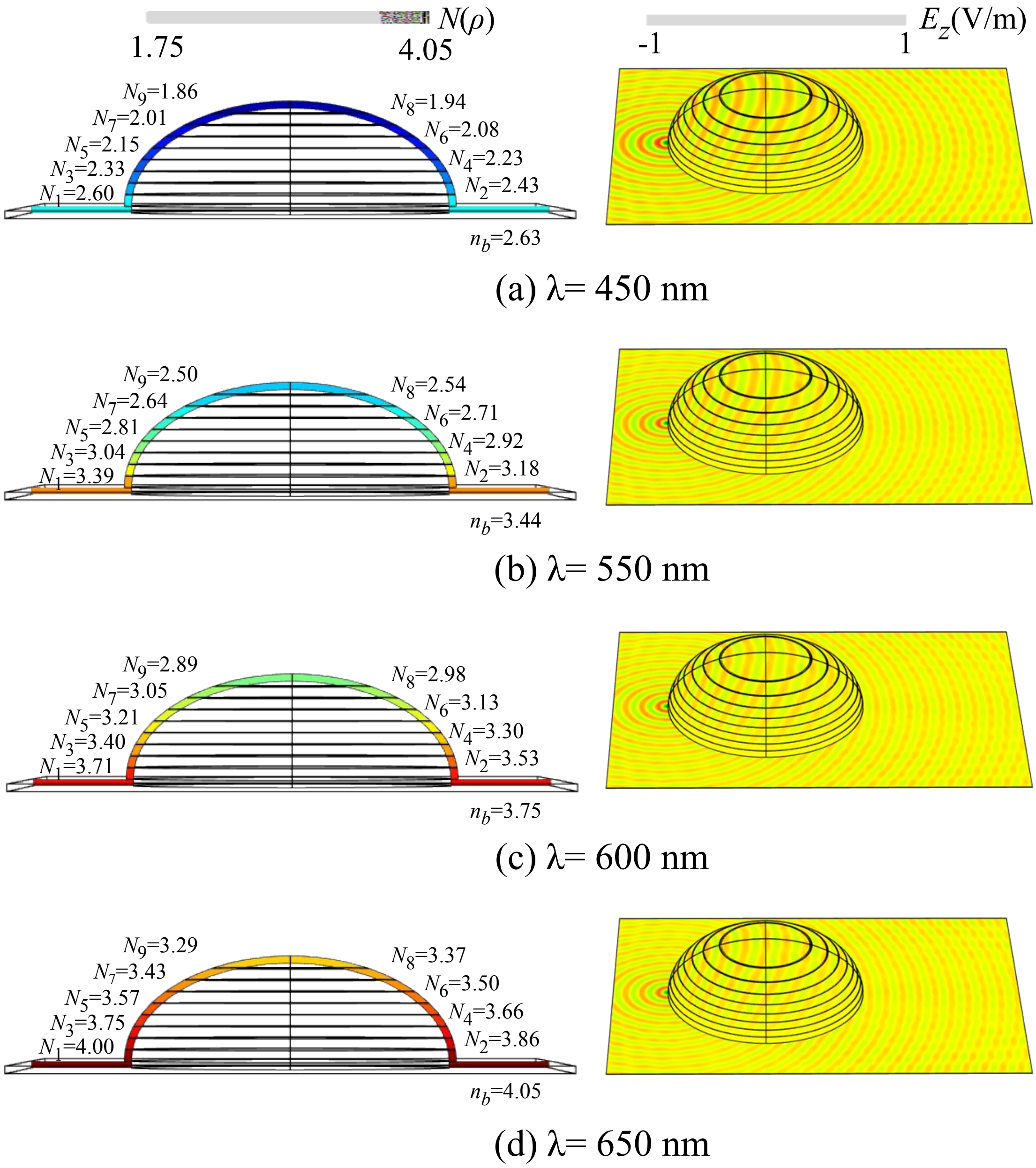

Figure S8. The propagation of E_z (left column) through the surface of 9-layered Rinehart-shaped curvature at (a) λ= 450 nm, (b) λ= 550 nm, (c) λ= 600 nm, and (d) λ= 650 nm, where the optical invisibility is imitated. The left column shows the radial cross sections of the discretized Rinehart-shaped surface at the different wavelengths.

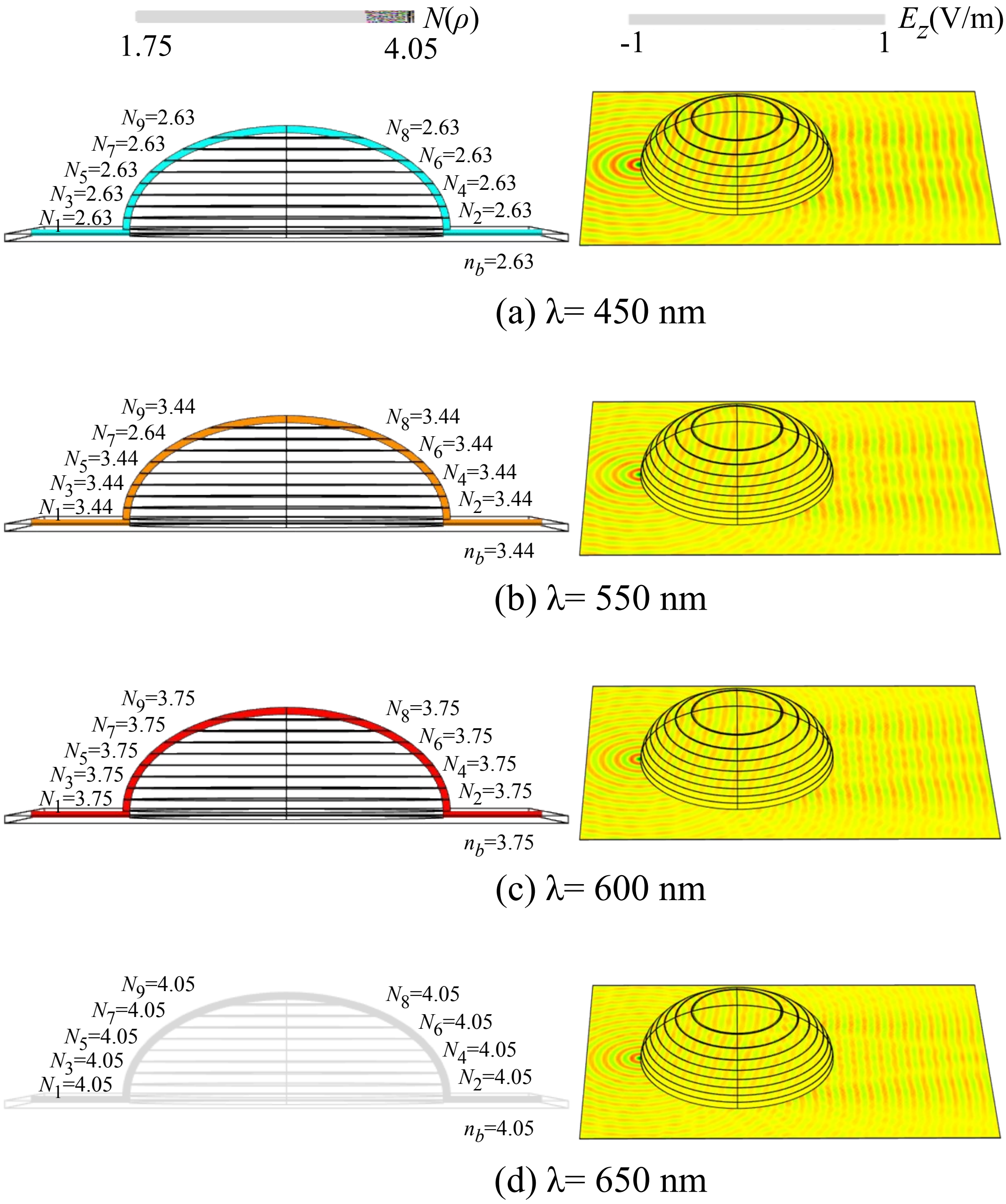

Figure S9. The propagation of E_z (left column) through the surface of 9-layered Rinehart-shaped curvature at (a) λ= 450 nm, (b) λ= 550 nm, (c) λ= 600 nm, and (d) λ= 650 nm, where the Luneburg lens is obtained. The left column shows the radial cross sections of the discretized Rinehart-shaped surface at the different wavelengths.

Section 6. The conditions of the $Ge_2Sb_2Te_5$ slabs for the various functions.

Table S1. The corresponding crystallization proportion, time durations, and refractive index of each $Ge_2Sb_2Te_5$ slab for the invisible cloaking at λ= 500 nm

Layer	**Crystallization ratio**	**Time duration (ns)**	**Refractive index**
#Ground	0	0	3
#1	16.7%	8	2.85
#2	27.8%	14	2.75
#3	44.4%	22	2.6
#4	53.3%	26	2.52
#5	63.3%	31	2.43
#6	73.3%	37	2.34
#7	83.3%	42	2.25
#8	92.2%	46	2.17
#9	100%	50	2.10

Table S2. The corresponding crystallization proportion, time durations, and refractive index of each $Ge_2Sb_2Te_5$ slab for the Maxwell fish-eye lens λ= 500 nm

Layer	Crystallization ratio	Time duration (ns)	Refractive index
#Ground	100%	50	2.1
#1	100%	50	2.1
#2	97.2%	48	2.13
#3	93.4%	46	2.17
#4	87.3%	43	2.23
#5	79.3%	39	2.31
#6	67.9%	33	2.42
#7	53.5%	26	2.56
#8	36.3%	18	2.72
#9	0	0	3.0

Table S3. The corresponding crystallization proportion, time durations, and refractive index of each $Ge_2Sb_2Te_5$ slab for the Einstein ring at λ= 500 nm

Layer	Crystallization ratio	Time duration (ns)	Refractive index
#Ground	0	0	3
#1	98%	49	2.12
#2	98%	49	2.12
#3	97%	48	2.13
#4	97%	48	2.13
#5	95%	47	2.14
#6	92%	46	2.17
#7	89%	44	2.2
#8	84%	42	2.24
#9	76%	38	2.32

Section 7. Description of the supporting movie.

It shows that the wavefront of a guided wave propagating across the layered curvature can be dynamically modulated via the stream of t_{bias}. Our device possesses an excellent performance of the continuous reconfigurability and versatile reprogrammable functions. The dynamic variations of the refractive index and temperature of each $Ge_2Sb_2Te_5$ layer for the different functionalities are presented simultaneously. However in order to simplify the movie, we only plot out the temperature distributions of the #Ground layer, layer #1 and #9.